Biogeosciences Discuss., 11, 657–690, 2014
www.biogeosciences-discuss.net/11/657/2014/
doi:10.5194/bgd-11-657-2014

Biogeosciences Discussions
Open Access

Winter to summer evolution of pCO_2 in surface water and air–sea CO_2 flux in the seasonal ice zone of the Southern Ocean

D. Nomura[1,2], H. Yoshikawa-Inoue[3], S. Kobayashi[3], S. Nakaoka[4], K. Nakata[1,3], and G. Hashida[5]

[1]Institute of Institute of Low Temperature Science, Hokkaido University, Kita-19, Nishi-8, Kita-ku, Sapporo, Hokkaido 060-0819, Japan
[2]Japan Society for the Promotion of Science (JSPS), 6 Ichiban-cho, Chiyoda, Tokyo 102-8471, Japan
[3]Graduate School of Environmental Science and Faculty of Environmental Earth Science, Hokkaido University, Kita-10, Nishi-5, Kita-ku, Sapporo 060-0810, Japan
[4]National Institute for Environmental Studies, 16-2 Onogawa, Tsukuba, Ibaraki 305-0053, Japan
[5]National Institute of Polar Research, 10-3 Midori-cho, Tachikawa, Tokyo 190-8501, Japan

Received: 30 November 2013 – Accepted: 23 December 2013 – Published: 10 January 2014

Correspondence to: D. Nomura (daiki@lowtem.hokudai.ac.jp)

Published by Copernicus Publications on behalf of the European Geosciences Union.

Abstract

Partial pressure of CO_2 (pCO_2) in surface water and vertical profiles of the aqueous carbonate system were measured during austral summer in the Indian sector of the Southern Ocean (64–67° S, 32–58° E) in January 2006 to understand the CO_2 dynamics of seawater in the seasonal ice zone. Surface-water pCO_2 ranged from 275 to 400 µatm, and longitudinal variations reflected the dominant influence of water temperature and dilution by sea-ice meltwater between 32° and 40° E and biological productivity between 40° and 58° E. Using carbonate system data from the temperature minimum layer, we examined the winter-to-summer evolution of surface-water pCO_2 and the factors affecting it. Our results indicate that pCO_2 increased by as much as 32 µatm, resulting mainly from the increase in water temperature. In synchrony with changes in sea ice concentration and surface-water pCO_2, air–sea CO_2 flux with considering the exchange of CO_2 between sea ice and atmosphere, changed from −1.1 to +0.9 mmol C m^{-2} day^{-1} between winter and summer. These results suggest that for the atmosphere, the seasonal ice zone acts as a CO_2 sink in winter and a CO_2 source in summer immediately after ice melt. Subsequent biological productivity likely decreases surface-water pCO_2 and air–sea CO_2 flux becomes negative, such that in summer the study area is a CO_2 sink with respect to the atmosphere.

1 Introduction

The Southern Ocean is the site of a large CO_2 flux between the sea and the air because of its large surface area and strong regional winds (Sabine and Key, 1998). Furthermore, water formed in the Southern Ocean ventilates the intermediate and abyssal depths of much of the world ocean (Rintoul and Bullister, 1999). Limited seasonal observations show that the air–sea CO_2 flux in the Southern Ocean varies over a wide range reflecting its oceanographic complexity (e.g. Takahashi et al., 2009). Recently, McNeil et al. (2007) computed a total CO_2 uptake of −0.4 Gt C yr^{-1} by the Southern

BGD
11, 657–690, 2014

Ocean on the basis of CO_2 partial pressure (pCO_2) in surface water, calculated from carbonate system parameters in seawater that were parameterized separately for the summer and winter seasons as a function of temperature, salinity and nutrient levels. More recently, however, Takahashi et al. (2009) estimated a smaller CO_2 uptake of $-0.05\,\mathrm{Gt\,C\,yr^{-1}}$ by incorporating new pCO_2 data from the 2000s and from the seasonal ice zone (SIZ), where relatively high pCO_2 exists in the water under the ice (Bakker et al., 1997, 2008; Rubin et al., 1998; Bellerby et al., 2004) and where the release of CO_2 to the atmosphere is limited to small areas of open water (e.g. polynyas, leads and cracks) in the ice-covered area.

The SIZ is the region where sea ice covers the surface of the ocean in winter and melts in summer (Moore and Abbott, 2000). In the Southern Ocean, the SIZ covers a large area due to the large contribution of first-year sea ice to the total sea ice area (Comiso, 2003). The distribution of surface-water pCO_2 in the SIZ is characterized by large variability in space and time. In spring and summer, pCO_2 is reportedly to be either low (Rubin et al., 1998; Metzl et al., 1999, 2006; Chierici et al., 2004; Inoue and Ishii, 2005) or high (Bakker et al., 1997, 2008; Jabaud-Jan et al., 2004; Shim et al., 2006) in surface water as compared to the atmosphere. Ishii et al. (2002) reported that pCO_2 becomes lower in surface water than in the air after the retreat of sea ice.

In winter, both high and low surface-water pCO_2 relative to the atmosphere has been reported (Hoppema et al., 1995; Bakker et al., 1997; Rubin et al., 1998; Gibson and Trull, 1999; Stoll et al., 1999; Bellerby et al., 2004; Metzl et al., 2006; Takahashi et al., 2009). In general, mixing with high-pCO_2 deep water and community respiration create high surface-water pCO_2. Sea ice may inhibit the release of CO_2 from the sea surface to the atmosphere, although recent studies have proposed the possibility of gas exchange through the sea ice (Loose et al., 2009; Geilfus et al., 2012; Nomura et al., 2013a). Brine rejection during the formation of sea ice may also contribute to high pCO_2 (Nomura et al., 2006; Rysgaard et al., 2007). Observations of low surface-water pCO_2 during winter (e.g. Hoppema et al., 1995; Stoll et al., 1999) have been explained as a remnant of low-pCO_2 water formed during earlier seasons (Sweeney

BGD
11, 657–690, 2014

et al., 2000; Sweeney, 2003; Hales and Takahashi, 2004; Metzl et al., 2006; Takahashi et al., 2009). In general the literature depicts CO_2 dynamics in the SIZ as a complicated subject because of sparsity of samples and imprecision in the parameterizations for processes including eddy mixing, ice formation and melting, and biological processes (Takahashi et al., 2012).

This study investigated the dynamics of CO_2 in seawater and its interaction with the atmosphere on the basis of surface-water pCO_2 data and the vertical profile of carbonate systems in the SIZ in the Indian sector of the Southern Ocean, measured in January (austral summer) of 2006. We used data from vertical profiles of carbonate system parameters in the temperature minimum layer to analyze changes in the surface-water pCO_2 and evaluate their relation to pCO_2 dynamics of the surface water and air–sea CO_2 flux.

2 Methods

We sampled from the R/V *Umitaka-Maru* in the Indian sector of the Southern Ocean (64–67° S, 32–58° E) from 12 to 19 January 2006 (Fig. 1 and Table 1). Stations L1–8 were far from the coast, and station FG3 was near the coast of Antarctica (Fig. 1).

During the cruise, pCO_2 in surface water was evaluated through the underway water measuring system (Inoue and Ishii, 2005; Nakaoka et al., 2009). CO_2 concentration (mole fraction of CO_2 in air; xCO_2) was measured quasi-continuously in air equilibrated with seawater using an automated CO_2 measuring system (Nippon ANS Co. Ltd., Tokyo, Japan). Seawater was taken continuously from a depth of about 10 m and introduced into the shower-type equilibrator (Inoue and Ishii, 2005). A non-dispersive infrared gas analyzer (Model 800, LI-COR, Inc., Lincoln, NE, USA) was used as the detector for CO_2 concentration measurements. The analyzer was calibrated every 1 h with four CO_2 standards (200, 266, 320 and 400 ppm) traceable to the World Meteorological Organization mole fraction scale (Inoue and Ishii, 2005). Atmospheric CO_2 concentration taken through a Teflon tube from the ship's mast was measured by the

BGD
11, 657–690, 2014

same manner as CO_2 concentration in surface water. pCO_2 was calculated from xCO_2 taking into account the water vapor pressure and atmospheric pressure.

Sea surface temperature (SST) and salinity (SSS) were measured continuously with a CT sensor (Falmouth Scientific, Inc., Cataumet, MA, USA) that was calibrated before and after the cruise by the manufacturer. Sea surface fluorescence was measured with a fluorescence probe (WETStar, WETLabs Inc., Philomath, OR, USA) at an inlet of the equilibrator. The fluorescence was converted to the chlorophyll *a* concentration based on the relationships between fluorescence and chlorophyll *a* concentration determined by a fluorometer (Model 10AU, Turner Designs, Inc., Sunnyvale, CA, USA) on the same water sample.

Vertical profiles of temperature and salinity were collected with a conductivity–temperature–depth (CTD) probe (SBE 911 plus, Sea-Bird Electronics, Bellevue, WA, USA) that was calibrated before and after the cruise by the manufacturer. Salinity data were also calibrated with bottle samples. Seawater samples were collected vertically in rosette-mounted 10 L Niskin bottles (General Oceanics, Inc, Miami, FL, USA). Seawater was subsampled into a 120 mL amber glass vial (Maruemu Co., Ltd., Osaka, Japan) for determination of dissolved inorganic carbon (DIC) and total alkalinity (TA), and into a 500 mL Nalgene polycarbonate bottle (Thermo Fisher Scientific, Inc., Waltham, MA, USA) for determination of chlorophyll *a* concentration. Immediately after DIC and TA sampling, a saturated mercury chloride ($HgCl_2$) solution (100 µL) was added to stop biological activity. Samples for measurement of DIC and TA were stored in a refrigerator at 4 °C until analysis. Samples for chlorophyll *a* measurement were immediately filtered through 25 mm Whatman GF/F filters, and chlorophyll pigments on the filters were extracted in dimethylformamide for 24 h in a deep freezer (−80 °C) (Suzuki and Ishimaru, 1990).

DIC was determined by coulometry (Johnson et al., 1999) using a coulometer (CM5012, UIC, Inc., Binghamton, NY, USA). The precision of DIC analysis from duplicate determinations is within ±0.1 % (Wakita et al., 2003). TA was determined by the improved single-point titration method (Culberson et al., 1970) using a pH meter

BGD
11, 657–690, 2014

(PHM240, Radiometer Analytical, Lyon, France). The precision of the TA analysis from duplicate determinations is within ±0.2 % (Wakita et al., 2003). Measurements for DIC and TA were calibrated by using the Certified Reference Material distributed by A. G. Dickson of Scripps Institution of Oceanography. To correct for the effects of dilution and concentration on DIC and TA due to formation and melting of sea ice, DIC and TA data were normalized (*n*-DIC and *n*-TA) to a salinity of 34.25, the mean value of the temperature minimum layer. Chlorophyll *a* concentration was determined by fluorometry (Parsons et al., 1984).

3 Results

3.1 Longitudinal distribution of pCO_2 SST, SSS and chlorophyll *a* concentration

Surface-water pCO_2 ranged from 275 to 399 µatm, and mean air pCO_2 was 366 µatm (Fig. 2a). Most pCO_2 in surface water was lower than that of air in the area between 38° and 58° E. Surface-water pCO_2 decreased from 377 µatm at 32° E to 275 µatm at 44° E, then increased to 340 µatm at 58° E. Chlorophyll *a* concentrations ranged from 0.2 to 0.9 $\mu g L^{-1}$ (Fig. 2b), reaching their maximum at 42.5° E. SST ranged from −1.5 to +1.2 °C and was generally low in the areas of 33–40° E and 45–58° E (Fig. 2c). SSS ranged from 32.5 to 34.1, reaching its minimum at 39° E (Fig. 2d).

3.2 Satellite images of sea ice and chlorophyll *a* concentrations

Temporal images of the sea ice concentration near sampling stations (Fig. 3) were derived from passive microwave imagery from the Advanced Microwave Scanning Radiometer–Earth Observing System (AMSR–E) (http://nsidc.org/data/amsre/). Before the middle of December 2005, the area near the sampling stations was > 80 % covered by sea ice (Fig. 3a–d). At the end of December 2005, sea ice areas decreased from north to south (Fig. 3e and f), and sea ice was at its minimum during our observation period in January 2006 (Fig. 3g and h). Sea ice concentration data for each

BGD
11, 657–690, 2014

station (Fig. 4a) corroborated this trend, and sea ice was absent north of stations L1–8. For station FG3, sea ice concentration began to decrease in early November 2005 and covered less than 80 % of the surface until the middle of December, when coverage grew again to 80 %. The sea-ice minimum occurred later here than at the other stations (Fig. 4a).

Temporal images of the chlorophyll *a* concentration near our sampling stations (Fig. 5) were derived from Sea-viewing Wide Field of view Sensor (SeaWiFS) data (http://oceancolor.gsfc.nasa.gov/SeaWiFS/). After sea ice had retreated, chlorophyll *a* concentrations near sampling stations increased, particularly near the ice edge (Figs. 4 and 5). At station FG3, a rapid increase of chlorophyll *a* was observed in early February (Fig. 4b). At the other stations, chlorophyll *a* concentration remained constant from January to March 2006.

3.3 Vertical profiles of temperature, salinity, *n*-DIC, *n*-TA and chlorophyll *a* concentration

For stations L1–8, vertical temperature profiles have a "C" shape, with higher temperatures above 30 m and below 100 m depth and lower temperatures between these depths (Fig. 6a). Salinity was low in the top 30 m, particularly at station L8 (32.5), and increased up to 34.7 with depth (Fig. 6b). The *n*-DIC was almost constant in the top 50 m of the water column (although different at each station), then increased down to 100 m depth (Fig. 6c). The *n*-TA decreased slightly with depth (Fig. 6d). Chlorophyll *a* concentration was low at the surface and below 130 m depth, although some stations had peaks up to 1.0 $\mu g L^{-1}$ deeper than 50 m (Fig. 6e).

For station FG3 near the coast of Antarctica, vertical profiles showed lower temperature, salinity and *n*-DIC and higher chlorophyll *a* concentration than at stations L1–8 (Fig. 6). For *n*-TA, profiles at all stations were similar (Fig. 6d).

BGD
11, 657–690, 2014

4 Discussion

The longitudinal distribution of pCO_2 in surface water varies with environmental factors. To understand the factors controlling surface-water pCO_2, we compared the pCO_2 distribution with chlorophyll *a*, SST and SSS. The chlorophyll *a* concentration was low ($0.2 \pm 0.0\,\mu g\,L^{-1}$) (mean +1 SD) between 32° and 40° E and high ($0.4 \pm 0.1\,\mu g\,L^{-1}$) between 40° and 58° E (Fig. 2b), demonstrating that the latter area was biologically productive. Figure 7 compares surface-water pCO_2 with SST for longitudes 32–40° E, 38–40° E (an area strongly affected by meltwater dilution) and 40–58° E. In 32–40° E, the increase in surface-water pCO_2 with SST was $14.4\,\mu atm\,^{\circ}C^{-1}$, or $3.9\,\%\,^{\circ}C^{-1}$ (Fig. 7a); this is close to the previously estimated value of $4.2\,\%\,^{\circ}C^{-1}$ due to thermodynamic effects (Takahashi et al., 2002). For the area strongly affected by freshwater input (Fig. 7b), pCO_2 decreased due to dilution by meltwater from sea ice, although surface-water pCO_2 was also dependent on SST ($4.6\,\%\,^{\circ}C^{-1}$). In 40–58° E (Fig. 7c), there was no significant relationship between surface-water pCO_2 and SST. In this biologically productive area, pCO_2 in surface water was apparently strongly affected by biological processes.

Previous studies in spring and summer have reported both low surface-water pCO_2 with respect to the atmosphere (Rubin et al., 1998; Metzl et al., 1999, 2006; Chierici et al., 2004; Inoue and Ishii, 2005) and high pCO_2 (Bakker et al., 1997, 2008; Jabaud-Jan et al., 2004; Shim et al., 2006). Ishii et al. (2002) reported that surface-water pCO_2 changed from higher to lower than atmospheric after the retreat of sea ice near our study area. Bakker et al. (2008) observed the same transition in the Weddell Gyre as ice-covered water gave way to biologically productive water.

Tomczak and Liefrink (2005) proposed that a water mass beneath the summer surface water with temperature between −1.9 °C and −1.5 °C and salinity between 34.2 and 34.5 constitutes the temperature minimum layer (TML). The TML is thought to retain the chemical characteristics of the surface mixed layer in winter (Ishii et al., 1998, 2002; Rubin et al., 1998; Hoppema and Goeyens, 1999; Pondaven et al., 2000). In

BGD
11, 657–690, 2014

our study area, the TML was at 50 m depth at stations L1–8 and at 200 m at station FG3 (Fig. 6). The higher temperature and lower salinity above the TML observed in our study (Fig. 6a and b) thus reflect warming from the atmosphere and freshening from melting sea ice.

In the TML, carbonate system parameters were nearly identical at all stations (2206.6±1.7 µmol kg^{-1} for *n*-DIC, 2327.6±2.1 µmol kg^{-1} for *n*-TA), and we treated these values as representative of winter conditions (n-DIC_{winter} and n-TA_{winter}). Surface-water pCO_2 in winter ($pCO_{2\,winter}$) was computed from n-DIC_{winter} and n-TA_{winter} at the freezing temperature of −1.8 °C using the program CO2SYS, version 01.05 (Lewis and Wallace, 1998). We used the carbonate dissociation constants (K_1 and K_2) of Mehrbach et al. (1973) as revised by Dickson and Millero (1987), and the K_{SO_4} determined by Dickson (1990). The resulting value of $pCO_{2\,winter}$ was 349.9 ± 6.4 µatm, which agrees well with the pCO_2 in winter derived from pCO_2–SST relationship (Fig. 7a).

Surface-water pCO_2 values in winter have been reported both above and below atmospheric values (Hoppema et al., 1995; Bakker et al., 1997; Rubin et al., 1998; Gibson and Trull, 1999; Stoll et al., 1999; Ishii et al., 2002; Bellerby et al., 2004; Metzl et al., 2006; Takahashi et al., 2009). High winter pCO_2 values in surface water have been ascribed to mixing with deep high-pCO_2 water and community respiration (Ishii et al., 2002; Bakker et al., 2008). Low winter values (305–331 µatm) typical of summer waters (Hoppema et al., 1995) have been explained as a remnant of low-pCO_2 water formed during earlier seasons (Sweeney et al., 2000; Sweeney, 2003; Hales and Takahashi, 2004; Metzl et al., 2006; Takahashi et al., 2009), and our calculated low $pCO_{2\,winter}$ in the surface water would be supported by these results.

Carbonate system parameters are changed by various processes, including biological (photosynthesis and respiration), gas exchange (CO_2 release and uptake) and carbonate mineral dissolution and formation (Anderson and Sarmiento, 1994; Zeebe and Wolf-Gladrow, 2001). A plot of *n*-DIC against *n*-TA in water above the TML (Fig. 8) suggests a complex mix of these processes. Stations L1 and FG3 appear to be governed by biological or gas exchange processes. The data establish regression lines

BGD
11, 657–690, 2014

with a slope of −0.1 for station L1 and −0.5 for station FG3, which are similar to those for biological (slope = −0.14) and gas exchange (slope = 0) processes. The areas around these stations were characterized by rapid ice melting and retreat (Figs. 3 and 4a), thereby starting gas exchange at the air–sea interface and promoting biological productivity at the ocean surface (Figs. 4 and 5). High chlorophyll *a* concentrations in vertical profiles (Fig. 6e) also reflected high biological productivity at the surface, particularly for station FG3.

For station L8, the slope of the regression line is 1.7 (Fig. 8), similar to that of the carbonate mineral process (slope = 2.0) for the precipitation of ikaite ($CaCO_3 \cdot 6H_2O$) during sea ice formation (Dieckmann et al., 2008; Nomura et al., 2013b) and its dissolution during the ice melting season (Rysgaard et al., 2013). The low salinity (32.5) at station L8 at the surface (Fig. 6b) is clear evidence of the influence of meltwater. Based on the change in salinity from 34.25 in winter to 32.5 in summer in the upper 20 m of the water column, we calculated a sea ice thickness of 1.0 m here in winter. The amount of ikaite in Antarctic sea ice has been estimated to be a maximum of 19.4 mg L^{-1} of meltwater equivalent (Dieckmann et al., 2008). Under the assumption that all ikaite in sea ice dissolved in the upper 20 m of the winter water column, meltwater input should alter *n*-DIC from 2206.6 µmol kg^{-1} to 2211.4 µmol kg^{-1} and *n*-TA from 2327.6 µmol kg^{-1} to 2337.2 µmol kg^{-1} during the transition from winter to summer at station L8. While ikaite formation and dissolution has been proposed as a contributor to changes of the carbonate system parameters during the ice melt season (Fransson et al., 2011; Rysgaard et al., 2013), the details are still poorly constrained and require further research (Nomura et al., 2013b). For the remaining stations (L2–7), a complex mixture of processes appears to be operating (Fig. 8).

We calculated the winter-to-summer evolution of surface-water pCO_2 in terms of four factors in the following equation (Bakker et al., 1997; Shim et al., 2006):

$$\Delta pCO_{2\,\text{water (winter to summer)}} = (\Delta pCO_{2\,\text{water}})T + (\Delta pCO_{2\,\text{water}})F + (\Delta pCO_{2\,\text{water}})B + (\Delta pCO_{2\,\text{water}})R \quad (1)$$

BGD
11, 657–690, 2014

where $\Delta pCO_{2\,\mathrm{water\,(winter\ to\ summer)}}$ is the pCO_2 change from winter (349.9 µatm) to summer (observed pCO_2), $(\Delta pCO_{2\,\mathrm{water}})\,T$ is the pCO_2 change from the temperature effect, $(\Delta pCO_{2\,\mathrm{water}})\,F$ is the pCO_2 change due to air–sea CO_2 flux, $(\Delta pCO_{2\,\mathrm{water}})\,B$ is the pCO_2 change from biological activity and $(\Delta pCO_{2\,\mathrm{water}})\,R$ is a residual term mainly reflecting upwelling, mixing, and variability of water masses including carbonate mineral dissolution/formation.

For the first term, we calculated the dependence of temperature on surface-water pCO_2 for each week, then summed these for the period from winter to summer:

$$(\Delta pCO_{2\,\mathrm{water}})T = \Sigma\left(\mathrm{d}pCO_{2\,\mathrm{water}}/\mathrm{d}t\right)T \quad (2)$$

where $(\mathrm{d}pCO_{2\,\mathrm{water}}/\mathrm{d}t)\,T$ was evaluated from the following equations (Takahashi et al., 2002):

$$(\mathrm{d}pCO_{2\,\mathrm{water}}/\mathrm{d}t)T = pCO_{2\,\mathrm{water}}(t_1) - pCO_{2\,\mathrm{water}}(t_0) \quad (3)$$

$$pCO_{2\,\mathrm{water}}(t_1) = pCO_{2\,\mathrm{water}}(t_0)\cdot[0.0423(T_{t1} - T_{t0})] \quad (4)$$

In these equations, t is time ($t_0 < t_1$) and T is the temperature of seawater in the 1° × 1° grid of optimal interpolation analysis data from Reynolds et al. (2002).

For the second term, we calculated the dependence of air–sea CO_2 flux on pCO_2 for every week, then summed these for the period from winter to summer:

$$(\Delta pCO_{2\,\mathrm{water}})F = \Sigma\mathrm{d}pCO_{2\,\mathrm{water}}/\mathrm{d}t)F \quad (5)$$

where $(\mathrm{d}pCO_{2\,\mathrm{water}}/\mathrm{d}t)$ F was evaluated as follows (Bakker et al., 1997):

$$(\mathrm{d}pCO_{2\,\mathrm{water}}/\mathrm{d}t)F = \beta\cdot pCO_{2\,\mathrm{water}}(F_{CO_2}/\mathrm{TDIC}) \quad (6)$$

where β is the buffer factor (we used the value of 14 from Takahashi et al., 1993), F_{CO_2} is the CO_2 flux between air and water, and TDIC is the total amount of DIC between

BGD
11, 657–690, 2014

the surface and the top of the TML. To calculate F_{CO_2}, we used the following equation:

$$F_{CO_2} = k \cdot s(pCO_{2\,air} - pCO_{2\,water}) \cdot (1 - S)/100 \quad (7)$$

$$k = 0.26u^2(Sc/660)^{-0.5} \quad (8)$$

where k is the gas transfer velocity (Wanninkhof, 1992; Takahashi et al., 2009), s is the gas solubility (Weiss, 1974), $pCO_{2\,air}$ is the atmospheric pCO_2 (366 µatm), S is the sea ice concentration, u is the wind speed (Kalnay et al., 2006), and Sc is the Schmidt number (Wanninkhof, 1992).

For the third term, we calculated the contribution of the biological effect on surface-water pCO_2 for the period from winter to summer:

$$(\Delta pCO_{2\,water})B = -\beta \cdot pCO_{2\,water\,(winter)}(NCP/TDIC) \quad (9)$$

where $pCO_{2water(winter)}$ is winter pCO_2 in surface water (349.9 µatm) and NCP is the net community production, evaluated as follows:

$$NCP = -\int_0^{Z_{T_{min}}} [(n\text{-}DIC(z) - n\text{-}DIC_{TML})S(z)\rho(z)/34.25]dz \quad (10)$$

where $Z_{T_{min}}$ is the depth of the top of the TML, n-DIC (z) is the value of n-DIC at depth z, n-DIC_{TML} is the value of n-DIC in the TML, and $S(z)$ and $\rho(z)$ are respectively the salinity and density of seawater at depth z.

Table 2 summarizes the resulting contributions of temperature, air–sea gas exchange and biological effects on the winter-to-summer evolution of surface-water pCO_2 for each station. Between winter and summer, the surface-water pCO_2 for stations L1–8 increased by 15.4 to 42.0 µatm (positive $\Delta pCO_{2\,water\,(winter\ to\ summer)}$), and the contribution of temperature was dominant (30.4–40.9 µatm). Surface-water pCO_2 for station FG3 decreased by 13.2 µatm (negative $\Delta pCO_{2\,water\,(winter\ to\ summer)}$), and biological production was the greatest contributor (−23.8 µatm) for negative ΔpCO_2. The NCP value

BGD
11, 657–690, 2014

($13.5\,g\,C\,m^{-2}$) at station FG3 was the highest among all stations, supporting this result. The high chlorophyll *a* concentrations near station FG3 (Figs. 2b, 4b and 5) are also consistent with this result. A previous study reported even higher NCP values, up to $34\,g\,C\,m^{-2}$, in this area in February (Ishii et al., 1998). Station L8 had a smaller value of $\Delta pCO_{2\,\text{water (winter to summer)}}$ (15.4 µatm) than stations L1–7, and there the contribution of the fourth, residual factor was especially high. Given the low salinity of surface water at station L8 (Fig. 6b), we believe that the residual factor mainly reflects the effects of meltwater containing carbonates on surface-water pCO_2.

Taken together, our results suggest that the seasonal increase of surface-water pCO_2 is mainly caused by the increase in water temperature from winter to summer in the area of stations L1–8 (Table 2). For station FG3, biological productivity is the dominant factor (Table 2). Figure 9 is a graph of the calculated seasonal relationships between parameters in the SIZ in our study area as represented by stations L1–8. With the summer rise in SST, surface-water pCO_2 rises above atmospheric levels in late December (Fig. 9a). Although we did not document it during our observation period, biological productivity in the study area should increase, as we observed at station FG3 (Figs. 4b, 5, 6e), after the retreat of sea ice (Fig. 9b). This development would trigger the depression of surface-water pCO_2 reported by Ishii et al. (1998) and Bakker et al. (2008).

We examined the longitudinal distribution of pCO_2 (Fig. 2a) to evaluate the thermodynamic dependence of surface-water pCO_2 in the study area (Fig. 10), using the difference between calculated and observed pCO_2 ($pCO_{2\,\text{cal.}} - pCO_{2\,\text{obs.}}$). We computed $pCO_{2\,\text{cal.}}$ from $n\text{-DIC}_{\text{winter}}$ and $n\text{-TA}_{\text{winter}}$ at the observed SST and SSS using the program CO2SYS. Therefore, the difference between $pCO_{2\,\text{cal.}}$ and $pCO_{2\,\text{obs.}}$ reflects the thermodynamic effect on surface-water pCO_2 from winter to summer. This difference was near zero ($+0.5 \pm 7.5$ µatm) between 32° and 40° E and as large as +100 µatm ($+47.5 \pm 16.3$ µatm) between 40° and 58° E (Fig. 10). These results suggest that the thermodynamic effect was dominant in 32–40° E. The positive excursion of this pCO_2

BGD
11, 657–690, 2014

differential in 40–58° E would be explained by biological productivity (Fig. 2b), which would reduce $pCO_{2\,obs.}$.

Air–sea CO_2 flux also changed in synchrony with the variations of surface-water pCO_2 and sea ice concentration (Fig. 9). In Eq. (7), we treated sea ice as a barrier to CO_2 exchange between air and sea. Therefore, air–sea CO_2 flux was defined as zero until sea ice concentration decreased in late December, when surface water was an early CO_2 source to the atmosphere as sea ice retreated, leading to air–sea CO_2 fluxes as great as $+0.9\,mmol\,C\,m^{-2}\,day^{-1}$ (Fig. 9b). Subsequently, photosynthesis and carbonate dynamics in sea ice meltwater lowered surface-water pCO_2 to the point that the water became a CO_2 sink. Our air–sea CO_2 fluxes (0.0 to $+0.9\,mmol\,C\,m^{-2}\,day^{-1}$) fall within the range (-8.2 to $+7.2\,mmol\,C\,m^{-2}\,day^{-1}$) reported in previous studies in the SIZ (Bakker et al., 1997; Metzl et al., 1999, 2006; Chierici et al., 2004; Nakaoka et al., 2009).

Although our estimate treated sea ice as impermeable to CO_2 exchange, recent studies have proposed that CO_2 exchange occurs through sea ice (Semiletov et al., 2004; Delille, 2006; Nomura et al., 2006, 2010a, b, 2013a; Zemmelink et al., 2006; Loose et al., 2009; Miller et al., 2011; Geilfus et al., 2012). Early during the period of ice growth, brines in sea ice attain high pCO_2 with decreasing temperature and increasing salinity (e.g., Papadimitriou et al., 2003). Thus, brine channels can emit CO_2 to the overlying air and, if the ice permeability is sufficiently high, to the overlying atmosphere (Delille, 2006; Nomura et al., 2006, 2010b; Loose et al., 2009; Miller et al., 2011a; Geilfus et al., 2012). And during the period of ice melt, sea-ice brine may take up atmospheric CO_2 because it has lower pCO_2 than the atmosphere due to algal productivity and dilution by meltwater (Semiletov et al., 2004; Delille, 2006; Zemmelink et al., 2006; Nomura et al., 2010a, 2013a). We incorporated this component as follows, using recent observations of Antarctic and Arctic sea ice (Nomura et al., 2013a):

$$\text{Air–ice–sea } F_{CO_2} = k \cdot s(pCO_{2\,air} - pCO_{2\,water}) \cdot (1 - S)/100 - F_{ice} \cdot S/100 \quad (11)$$

BGD
11, 657–690, 2014

where air–ice–sea F_{CO_2} is the flux including air–sea ice CO_2 flux (F_{ice}) in addition to the air–sea CO_2 flux as calculated in Eq. (7). Because sea ice melts and becomes flooded during seasonal warming even while sea ice concentration is still high, we used the value $-1.1 \pm 0.9\,\mathrm{mmol\,C\,m^{-2}\,day^{-1}}$ for F_{ice} taken from direct measurements by the chamber technique over the melting and flooded sea ice surface (Nomura et al., 2013a). This value was within the range (-5.2 to $+0.9\,\mathrm{mmol\,C\,m^{-2}\,day^{-1}}$) reported by previous studies using the chamber method (Delille, 2006; Nomura et al., 2010a, b; Geilfus et al., 2012). Our calculations show that air–sea ice CO_2 flux was dominant until sea-ice retreat beginning in December, when the positive air–sea CO_2 flux overcame it and the net CO_2 flux to the air became positive, reaching about $+0.8\,\mathrm{mmol\,C\,m^{-2}\,day^{-1}}$ after the sea ice disappeared (Fig. 9b).

It has been argued that leads, cracks and polynyas within the sea ice area are hot spots for gas exchange between the air and surface water (Zemmelink et al., 2008; Else et al., 2013; Steiner et al., 2013). However, formation of surface melt ponds (Semiletov et al., 2004) and carbon uptake by algae within them (Lee et al., 2012) can also contribute to CO_2 uptake. Even without considering meltwater, the presence of snow on sea ice also affects the CO_2 flux (Nomura et al., 2010a, 2013a). For accurate calculation of CO_2 flux in the SIZ, it is clear that in addition to the open ocean surface, ice areas are influential in the carbon and biogeochemical cycles of polar seas.

The results of this study shed light on CO_2 dynamics and flux during the winter-to-summer transition in the SIZ. However, it is not yet certain whether the SIZ acts as a CO_2 sink or source for the atmosphere through this season. This study evaluated the air–sea CO_2 flux (including air–ice CO_2 flux) as negative in winter, indicating a CO_2 sink (Fig. 9a). Although sea ice blocks the direct exchange of CO_2 between the ocean and atmosphere, pCO_2 in the water under the ice (349.9 µatm) is low with respect to the atmosphere (Fig. 9a), suggesting that water in the SIZ is a potential sink in winter in addition to the direct CO_2 absorption by the sea ice surface (Nomura et al., 2013a). Ishii et al. (2002), however, reported that pCO_2 in surface water (390 µatm) is high in winter with respect to the atmosphere near our study area and that CO_2 could enter

BGD
11, 657–690, 2014

the atmosphere (indicating a CO_2 source) through ice-free regions such as polynyas and leads. Further studies are needed to address these conflicting findings.

Acknowledgements. We thank the crew of R/V *Umitaka-Maru* and cruise members for their support in conducting the field work. This work was partly supported by the Japan Society for the Promotion of Science (23241002) and the National Institute of Polar Research.

References

Anderson, L. A. and Sarmiento, J. L.: Redfield ratios of remineralization determined by nutrient data analysis, Global Biogeochem. Cy., 8, 65–80, 1994.

Bakker, D. C. E., de Baar, H. J. W., and Bathmann, U. V.: Changes of carbon dioxide in surface waters during spring in the Southern Ocean, Deep-Sea Res. Pt. II, 44, 91–127, 1997.

Bakker, D. C. E., Hoppema, M., Schröder, M., Geibert, W., and de Baar, H. J. W.: A rapid transition from ice covered CO_2-rich waters to a biologically mediated CO_2 sink in the eastern Weddell Gyre, Biogeosciences, 5, 1373–1386, doi:10.5194/bg-5-1373-2008, 2008.

Bellerby, R. G. J., Hoppema, M., Fahrbach, E., De Baar, H. J. W., and Stoll, M. H. C.: Interannual controls on Weddell Sea surface water fCO_2 during the autumn–winter transition phase, Deep-Sea Res. Pt. I, 51, 793–808, 2004.

Chierici, M., Fransson, A., Turner, D. R., Pakhomov, E. A., and Froneman, P. W.: Variability in pH, fCO_2, oxygen and flux of CO_2 in the surface water along a transect in the Atlantic sector of the Southern Ocean, Deep-Sea Res. pt. II, 51, 2773–2787, 2004.

Comiso, J. C.: Large-scale characteristics and variability of the global sea ice cover, in: Sea Ice – An Introduction to Its Physics, Chemistry, Biology and Geology, edited by: Thomas, D. N. and Dieckmann, G. S., Blackwell Science, Oxford, 112–142, 2003.

Culberson, C., Pytkowicz, R. M., and Hawley, J. E.: Seawater alkalinity determination by the pH method, J. Mar. Res., 28, 15–21, 1970.

Delille, B.: Inorganic carbon dynamics and air–ice–sea CO_2 fluxes in the open and coastal waters of the Southern Ocean, Ph. D. thesis, Univ. of Liége, Liége, Belgium, 1–297, 2006.

Dickson, A. G.: Thermodynamics of the dissociation of boric acid in synthetic seawater from 273.15 to 318.15 K, Deep-Sea Res. Pt. I, 37, 755–766, 1990.

Dickson, A. G. and Millero, F. J.: A comparison of the equilibrium constants for the dissociation of carbonic acid in seawater media, Deep-Sea Res., 34, 1733–1743, 1987.

BGD
11, 657–690, 2014

Dieckmann, G. S., Nehrke, G., Papadimitriou, S., Göttlicher, J., Steininger, R., Kennedy, H., Wolf-Gladrow, D., and Thomas, D. N.: Calcium carbonate as ikaite crystals in Antarctic sea ice, Geophys. Res. Lett., 35, L08501, doi:10.1029/2008GL033540, 2008.

Else, B. G. T., Papakyriakou, T. N., Asplin, M. G., Barber, D. G., Galley, R. J., Miller, L. A., and Mucci, A.: Annual Cycle of Air–Sea CO_2 Exchange in an Arctic Polynya Region, Global Biogeochem. Cy., 27, 388–398, 2013.

Fransson, A., Chierici, M., Yager, P. L., and Smith Jr., W. O.: Antarctic sea ice carbon dioxide system and controls, J. Geophys. Res., 116, C12035, doi:10.1029/2010JC006844, 2011.

Geilfus, N.-X., Carnat, G., Papakyriakou, T., Tison, J.-L., Else, B., Thomas, H., Shadwick, E., and Delille, B.: Dynamics of pCO_2 and related air–ice CO_2 fluxes in the Arctic coastal zone (Amundsen Gulf, Beaufort Sea), J. Geophys. Res., 117, C00G10, doi:10.1029/2011JC007118, 2012.

Gibson, J. A. E. and Trull, T. W.: Annual cycle of fCO_2 under sea-ice and in open water in Prydz Bay, East Antarctica, Mar. Chem., 66, 187–200, 1999.

Hales, B. and Takahashi, T.: High-resolution biogeochemical investigation of the Ross Sea, Antarctica, during the AESOPS (US JGOFS) Program, Global Biogeochem. Cy., 18, GB3006, doi:10.1029/2003GB002165/full, 2004.

Hoppema, M. and Goeyens, L.: Redfield behavior of carbon, nitrogen, and phosphorus depletions in Antarctic surface water, Limnol. Oceanogr., 44, 1, 220–224, 1999.

Hoppema, M., Fahrbach, E., Schröder, M., Wisotzki, A., and de Baar, H. J. W.: Winter–summer difference of carbon dioxide and oxygen in the Weddell Sea surface layer, Mar. Chem., 51, 177–192, 1995.

Inoue, H. Y. and Ishii, M.: Variations and trends of CO_2 in the surface seawater in the Southern Ocean south of Australia between 1969 and 2002, Tellus B, 57, 58–69, 2005.

IPCC: Climate change 2007: the physical science basis, in: Contribution of Working Group I of the Fourth Assessment Report of the Intergovernmental Panel on Climate Change, edited by: Solomon, S., Quin, D., Manning, M., Chen, Z., Marquis, M., Averyt, K. B., Tignor, M., and Miller, H. L., Cambridge University Press, Cambridge, UK and New York, NY, USA, 996 pp., 2007.

Ishii, M., Inoue, H. Y., Matsueda, H., Tanoue, E.: Close coupling between seasonal biological production and dynamics of dissolved inorganic carbon in the Indian Ocean sector and the western Pacific Ocean sector of the Antarctic Ocean, Deep-Sea Res. Pt. I, 45, 1187–1209, 1998.

BGD
11, 657–690, 2014

Ishii, M., Inoue, H. Y., and Matsueda, H.: Net community production in the marginal ice zone and its importance for the variability of the oceanic pCO_2 in the Southern Ocean south of Australia, Deep-Sea Res. Pt. II, 49, 1691–1706, 2002.

Jabaud-Jan, A., Metzl, N., Brunet, C., Poisson, A., and Schauer, B.: Interannual variability of the carbon dioxide system in the southern Indian Ocean (20° S–60° S): the impact of a warm anomaly in austral summer 1998, Global Biogeochem. Cy., 18, B1042, doi:10.1029/2002GB002017, 2004.

Johnson, K. M., Körtzinger, A., Mintrop, L., Duinker, J. C., and Wallace, D. W. R.: Coulometric total carbon dioxide analysis for marine studies: measurements and internal consistency of underway TCO_2 concentrations, Mar. Chem., 67,123–144, 1999.

Kalnay, E., Kanamitsu, M., Kistler, R., Collins, W., Deaven, D., Gandin, L., Iredell, M., Saha, S., White, G., Woollen, J., Zhu, Y., Leetmaa, A., Reynolds, R., Chelliah, M., Ebisuzaki, W., Higgins, W., Janowiak, J., Mo, K. C., Ropelewski, C., Wang, J., Jenne, R., and Joseph, D.: The NCEP/NCAR 40 yr reanalysis project, B. Am. Meteorol. Soc., 77, 437–471, 1996.

Lee, S. H., Stockwell, D. A., Joo, H.-M., Son, Y., Kang, C.-K., and Whitledge, T. E. E.: Phytoplankton production from melting ponds on Arctic sea ice, J. Geophys. Res., 117, C4, doi:10.1029/2011JC007717, 2012.

Lewis, E. and Wallace, D. W. R.: Program Developed for CO_2 System Calculations, ORNL/CDIAC-105. Carbon Dioxide Information Analysis Center, Oak Ridge National Laboratory, US Department of Energy, Oak Ridge, TN, available at: http://cdiac.esd.ornl.gov/oceans/co2rprt.html, 1998.

Loose, B., McGillis, W. R., Schlosser, P., Perovich, D., and Takahashi, T.: Effects of freezing, growth, and ice cover on gas transport processes in laboratory seawater experiments, Geophys. Res. Lett., 36, 5, doi:10.1029/2008GL036318, 2009.

McNeil, B. I., Metzl, N., Key, R. M., Matear, R. J., and Corbiére, A.: An empirical estimate of the Southern Ocean air–sea CO_2 flux, Global Biogeochem. Cy., 21, GB3011, doi:10.1029/2007GB002991, 2007.

Mehrbach, C., Culberson, C. H., Hawley, J. E., and Pytkowicz, R. M.: Measurement of the apparent dissociation constants of carbonic acid in seawater at atmospheric pressure, Limnol. Oceanogr., 18, 897–907, 1973.

Metzl, N., Tilbrook, B., and Poisson, A.: The annual fCO_2 cycle and the air–sea CO_2 fluxes in the sub-Antarctic Ocean, Tellus, Ser. B, 51, 849–861, 1999.

BGD
11, 657–690, 2014

Metzl, N., Brunet, C., Jabaud-Jan, A., Poisson, A., and Schauer, B.: Summer and winter air–sea CO_2 fluxes in the Southern Ocean, Deep-Sea Res. Pt. I, 53, 1548–1563, 2006.

Miller, L. A., Papakyriakou, T. N., Collins, R. E., Deming, J. W., Ehn, J. K., Macdonald, R. W., Mucci, A., Owens, O., Raudsepp, M., and Sutherland, N.: Carbon dynamics in sea ice: a winter flux time series, J. Geophys. Res., 116, C02028, doi:10.1029/2009JC006058, 2011.

Moore, J. K. and Abbott, M. R.:. Phytoplankton chlorophyll distributions and primary production in the Southern Ocean, J. Geophys. Res., 105, 28709–28772, 2000.

Nakaoka, S., Nakazawa, T., Yoshikawa-Inoue, H., Aoki, S., Hashida, G., Ishii, M., Yamanouchi, T., Odate, T., and Fukuchi, M.: Variations of oceanic pCO_2 and air–sea CO_2 flux in the eastern Indian sector of the Southern Ocean for the austral summer of 2001–2002, Geophys. Res. Lett., 36, L14610, doi:10.1029/2009GL038467, 2009.

Nomura, D., Inoue, H. Y., and Toyota, T.: The effect of sea-ice growth on air–sea CO_2 flux in a tank experiment, Tellus, Ser. B, 58, 418–426, 2006.

Nomura, D., Inoue, H. Y., Toyota, T., and Shirasawa, K.: Effects of snow, snowmelting and refreezing processes on air–sea–ice CO_2 flux, J. Glaciol., 56, 196, 262–270, 2010a.

Nomura, D., Eicken, H., Gradinger, R., and Shirasawa, K.: Rapid physically driven inversion of the air–sea ice CO_2 flux in the seasonal landfast ice off Barrow, Alaska after onset of surface melt, Cont. Shelf Res., 30, 1998–2004, 2010b.

Nomura, D., Granskog, M. A., Assmy, P., Simizu, D., Hashida, G.: Arctic and Antarctic sea ice acts as a sink for atmospheric CO_2 during periods of snow melt and surface flooding, J. Geophys. Res., 118, doi:10.1002/jgrc.20430, 2013a.

Nomura, D., Assmy, P., Nehrke, G., Granskog, M. A., Fischer, M., Dieckmann, G. S., Fransson, A., Hu, Y., and Schnetger, B.: Characterization of ikaite ($CaCO_3 \cdot 6H_2O$) crystals in first-year Arctic sea ice north of Svalbard, Ann. Glaciol., 54, 125–131, doi:10.3189/2013AoG62A034, 2013b.

Papadimitriou, S., Kennedy, H., Kattner, G., Dieckmann, G. S., and Thomas, D. N.: Experimental evidence for carbonate precipitation and CO_2 degassing during sea ice formation, Geochim. Cosmochim. Ac., 68, 1749–1761, 2003.

Parsons, T. R., Takahashi, M., and Hargrave. B.: Biological Oceanographic Processes, 3rd edn., Pergamon, Oxford, U. K., 330 pp., 1984.

Pondaven, P., Ragueneau, O., Tréguer, P., Hauvespre, A., Dezileau, L., Reyss, J. L.: Resolving the “opal paradox” in the Southern Ocean, Nature, 405, 168–172, 2000.

BGD
11, 657–690, 2014

Reynolds, R. W., Rayner, N. A., Smith, T. M., Stokes, D. C., and Wang, W.: An improved in situ and satellite SST analysis for climate, J. Climate, 15, 1609–1625, 2002.

Rintoul, S. R. and Bullister, J. L.:. A late winter hydrographic section from Tasmania to Antarctica, Deep-Sea Res. Pt. I, 46, 1417–1454, 1999.

Rubin, S. I., Takahashi, T., Chipman, D. W., Goddard, J. G.: Primary productivity and nutrient utilization ratios in the Pacific sector of the Southern Ocean based on seasonal changes in seawater chemistry, Deep-Sea Res. Pt. I, 45, 1211–1234, 1998.

Rysgaard, S., Glud, R. N., Sejr, M. K., Bendtsen, J., and Christensen, P. B.: Inorganic carbon transport during sea ice growth and decay: a carbon pump in polar seas, J. Geophys. Res., 112, C03016, doi:10.1029/2006JC003572, 2007.

Rysgaard, S., Søgaard, D. H., Cooper, M., Pućko, M., Lennert, K., Papakyriakou, T. N., Wang, F., Geilfus, N. X., Glud, R. N., Ehn, J., McGinnis, D. F., Attard, K., Sievers, J., Deming, J. W., and Barber, D.: Ikaite crystal distribution in winter sea ice and implications for CO_2 system dynamics, The Cryosphere, 7, 707–718, doi:10.5194/tc-7-707-2013, 2013.

Sabine, C. L. and Key, R. M.: Controls on fCO_2 in the South Pacific, Mar. Chem., 60, 95–110, 1998.

Semiletov, I., Makshtas, S., Akasofu, S., and Andreas, E. L.: Atmospheric CO_2 balance: the role of Arctic sea ice, Geophys. Res. Lett., 31, doi:10.1029/2003GL017996, 2004.

Shim, J., Kang, Y. C., Kim, D., and Choi, S.: Distribution of net community production and surface pCO_2 in the Scotia Sea, Antarctica, during austral spring 2001', Mar. Chem., 101, 68–84, 2006.

Steiner, N., Lee, W. G., and Christian, J. R.: Enhanced gas fluxes in small sea ice leads and cracks: effects on CO_2 exchange and ocean acidification, J. Geophys. Res., 118, 1195–1205, 2013.

Stoll, M. H. C., de Baar, H. J. W., Hoppema, M., and Fahrbach, E.: New early winter fCO_2 data reveal continuous uptake of CO_2 by the Weddell Sea, Tellus B, 51, 679–687, 1999.

Suzuki, R. and Ishimaru, T.: An improved method for the deter-mination of phytoplankton chlorophyll using N, N-dimethylformamide, J. Oceanogr. Soc. Jpn., 46, 190–194, doi:10.1007/BF02125580, 1990.

Sweeney, C.: The annual cycle of surface CO_2 and O_2 in the Ross Sea: a model for gas exchange on the continental shelves of Antarctica, in: Biogeochemistry of the Ross Sea, edited by: DiTullio, G. R. and Dunbar, R. B., Antarct. Res. Ser., 78, 295–312, 2003.

BGD
11, 657–690, 2014

Sweeney, C., Smith, W. O., Hales, B., Bidigare, R. R., Carlson, C. A., Codispoti, L. A., Gordon, L. I., Hansell, D., Millero, F. J., Park, Mi.-O. K., and Takahashi, T.: Nutrient and carbon removal ratios and fluxes in the Ross Sea, Antarctica, Deep-Sea Res. Pt. II, 47, 3395–3421, 2000.

Takahashi, T., Olafsson, J., Goddard, J. G., Chipman, D. W., and Sutherland, S. C.: Seasonal variations of CO_2 and nutrients in the high-latitude surface oceans: a comparative study, Global Biogeochem. Cy., 7, 843–878, 1993.

Takahashi, T., Sutherland, S. C., Sweeny, C., Poisson, A., Metzl, N., Tilbrook, B., Nates, N., Wanninkhof, R., Feely, R. A., Sabine, C., Olafsson, J., and Nojiri, Y.: Global sea–air CO_2 flux based on climatological surface ocean pCO_2 and seasonal biological and temperature effects, Deep-Sea Res. Pt. II, 49, 1601–1622, 2002.

Takahashi, T., Sutherland, S. C., Wanninkhof, R., Sweeney, C., Feely, R. A., Chipman, D. W., Hales, B., Friederich, G., Chavez, F., Sabine, C., Watson, A., Bakker, D. C. E., Schuster, U., Metzl, N., Yoshikawa-Inoue, H., Ishii, M., Midorikawa, T., Nojiri, Y., Körtzinger, A., Steinhoff, T., Hoppema, M., Olafsson, J., Arnarson, T. S., Tilbrook, B., Johannessen, T., Olsen, A., Bellerby, R., Wong, C. S., Delille, B., Bates, N. R., and de Baar, H. J. W.: Climatological mean and decadal change in surface ocean pCO_2, and net sea–air CO_2 flux over the global oceans, Deep-Sea Res. Pt. II, 56, 554–577, 2009.

Takahashi, T., Sweeney, C., Hales, B., Chipman, D. W., Newberger, T., Goddard, J. G., Iannuzzi, R. A., and Sutherland, S. C.: The changing carbon cycle in the Southern Ocean, Oceanography, 25, 26–37, 2012.

Tomczak, M. and Liefrink, S.: Interannual variations of water mass volumes in the Southern Ocean, J. Atmos. Ocean Sci., 10, 31–42, 2005, http://www.ocean-sci.net/10/31/2005/.

Wakita, M., Watanebe, W. Y., Watanebe, S., and Noriki, S.: Oceanic uptake rate of anthropogenic CO_2 in a subpolar marginal sea: the Sea of Okhotsk, Geophys. Res. Lett., 30, 24, doi:10.1029/2003GL018057, 2003.

Wanninkhof, R.: Relationship between wind speed and gas exchange over the ocean, J. Geophys. Res., 97, 7373–7382, 1992.

Weiss, R. F.:. Carbon dioxide in water and seawater: the solubility of a non-ideal gas, Mar. Chem., 2, 203–205, 1974.

Zeebe, R. E. and Wolf-Gladrow, D.: CO_2 in Seawater: Equilibrium, Kinetics, Isotopes, Elsevier Oceanogr. Ser. 65, Elsevier, Amsterdam, 2001.

BGD
11, 657–690, 2014

Zemmelink, H. J., Delille, B., Tison, J.-L., Hintsa, E. J., Houghton, L., and Dacey, J. W. H.: CO_2 deposition over the multi-year ice of the western Weddell Sea, Geophys. Res. Lett., 33, L13606, doi:10.1029/2006GL026320, 2006.

Zemmelink, H. J., Houghton, L., Dacey, J. W. H., Stefels, J., Koch, B. P., Schröder, M., Wisotzki, A., Scheltz, A., Thomas, D. N., Papadimitriou, S., Kennedy, H., Kuosa, H., and Dittmar, T.: Stratification and the distribution of phytoplankton, nutrients, inorganic carbon and sulfur in the surface waters of Weddell Sea leads, Deep-Sea Res. Pt. II, 55, doi:10.1016/j.dsr2.2007.12011, 2008.

BGD
11, 657–690, 2014

Table 1. Sampling dates, times (UTC) and locations of CTD stations.

Station	Date of 2006	Time	Latitude (° S)	Longitude (° E)
L1	13 Jan	10:23	65.0	36.0
L2	13 Jan	3:31	65.3	36.0
L3	12 Jan	22:25	65.7	36.0
L4	12 Jan	3:49	66.2	36.0
L5	14 Jan	16:59	65.0	38.0
L6	14 Jan	22:36	65.3	38.0
L7	15 Jan	3:41	65.7	38.0
L8	16 Jan	3:30	66.9	37.9
FG3	19 Jan	7:19	65.9	51.4

BGD
11, 657–690, 2014

Table 2. Contributions of temperature (($\Delta pCO_{2\,water}$) T), air–sea flux (($\Delta pCO_{2\,water}$) F), biological production (($\Delta pCO_{2\,water}$) B) and residual mechanisms (($\Delta pCO_{2\,water}$) R) to the winter-to-summer evolution of surface-water pCO_2 ($\Delta pCO_{2\,water\,(winter\ to\ summer)}$) for each station.

Station	$\Delta pCO_{2\,water\,(winter\ to\ summer)}$	($\Delta pCO_{2\,water}$) T	($\Delta pCO_{2\,water}$) F	($\Delta pCO_{2\,water}$) B	($\Delta pCO_{2\,water}$) R
L1	42.0	38.6	–0.1	–9.2	12.8
L2	38.3	34.7	–0.1	–[a]	3.8
L3	39.8	34.7	–0.2	–6.3	11.6
L4	30.1	30.4	0.0	–[a]	–0.2
L5	39.7	39.6	–0.2	–[a]	0.5
L6	40.7	40.9	–0.6	–5.2	5.6
L7	42.0	40.9	–0.7	–[a]	1.9
L8	15.4	33.9	0.0	–[a]	–18.4
FG3	–13.2	24.3	0.1	–23.8	–15.2

[a] No data due to no significant difference of *n*-DIC between surface and the upper part of the TML for NCP calculation. NCP was 2.5 g C m^{-2} for station L1, 1.7 g C m^{-2} for station L3, 1.5 g C m^{-2} for station L6 and 13.5 g C m^{-2} for station FG3.

BGD
11, 657–690, 2014

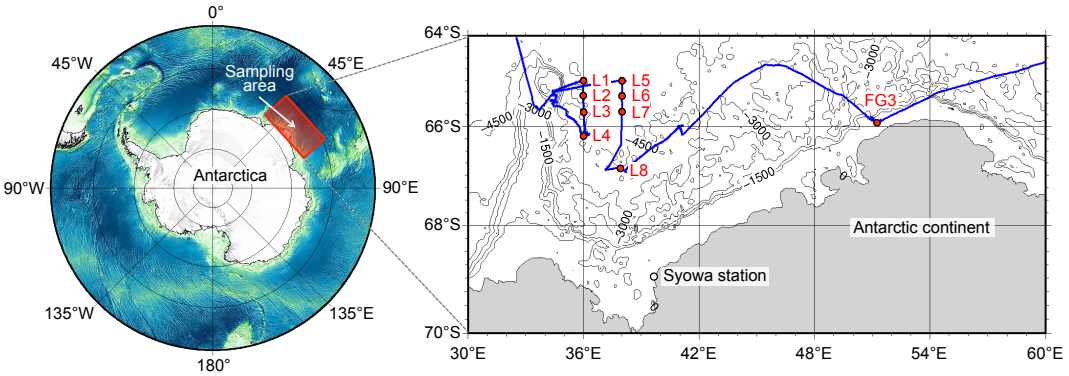

Fig. 1. Location map of the sampling area in the Indian sector of the Southern Ocean showing the cruise track (blue line) and CTD station locations (red circles). Bathymetric contours are at 750 m intervals.

BGD
11, 657–690, 2014

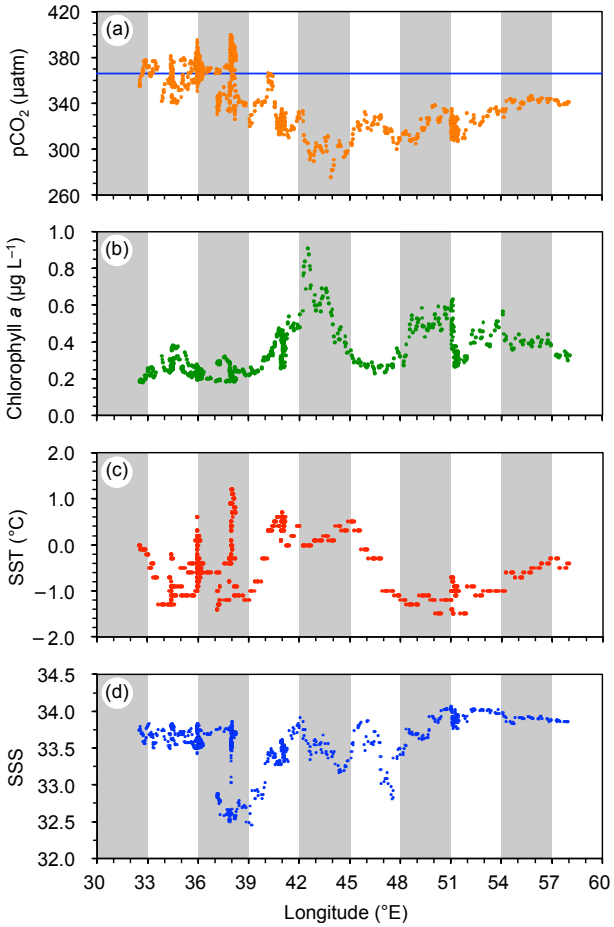

Fig. 2. Longitudinal distribution of surface-water pCO_2 **(a)**, chlorophyll *a* **(b)**, SST **(c)** and SSS **(d)**. Blue line in **(a)** indicates atmospheric pCO_2.

BGD
11, 657–690, 2014

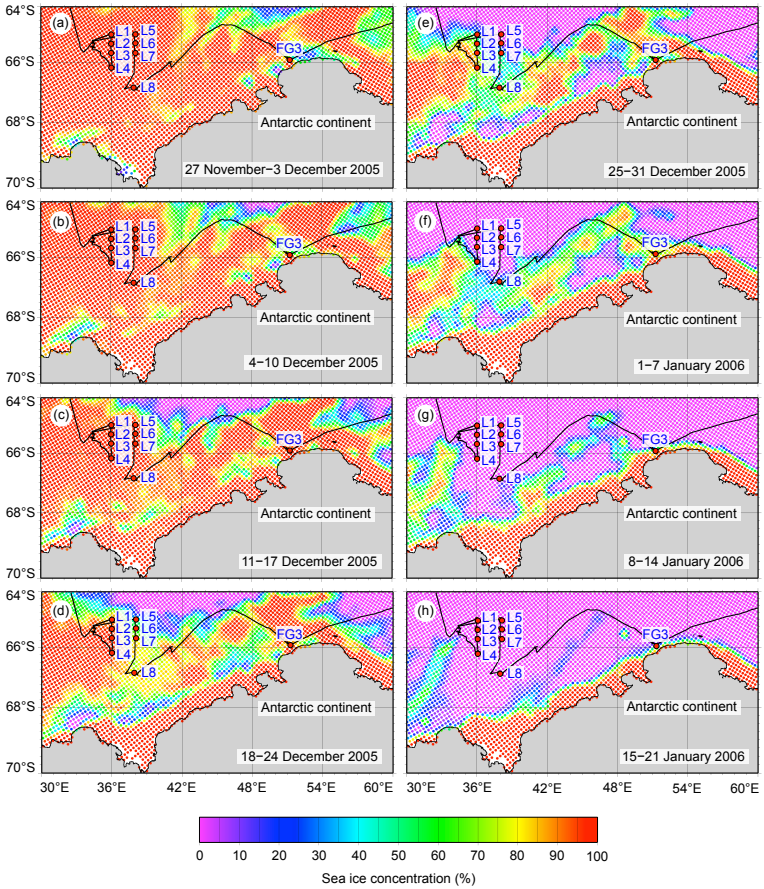

Fig. 3. Weekly mean sea ice concentration in the study area for 27 November–3 December 2005 **(a)**, 4–10 December 2005 **(b)**, 11–17 December 2005 **(c)**, 18–24 December 2005 **(d)**, 25–31 December 2005 **(e)**, 1–7 January 2006 **(f)**, 8–14 January 2006 **(g)** and 15–21 January 2006 **(h)**. Images derived from AMSR-E satellite data.

BGD
11, 657–690, 2014

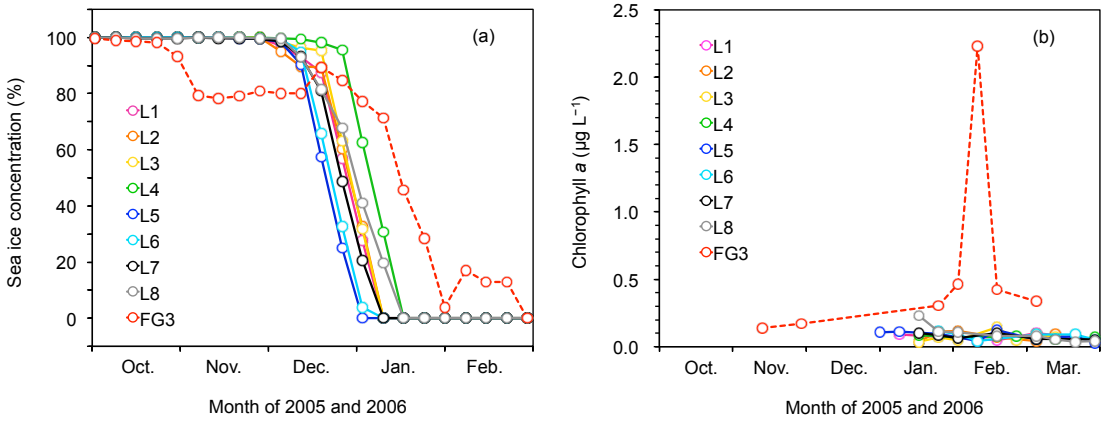

Fig. 4. Seasonal variations in sea ice concentration from AMSR-E data **(a)** and chlorophyll *a* concentration from SeaWIFS data **(b)**.

BGD
11, 657–690, 2014

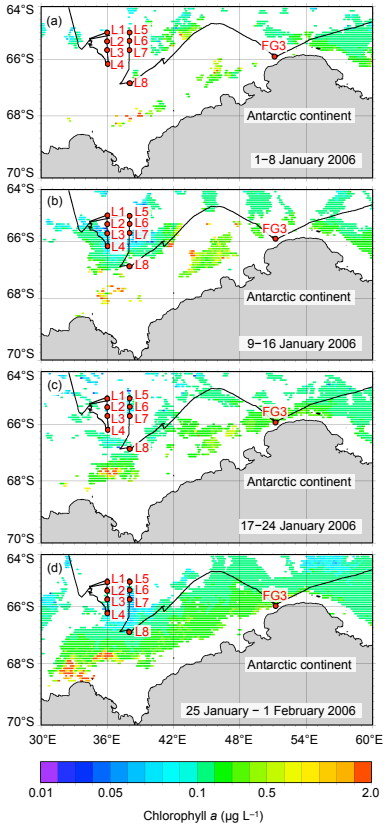

Fig. 5. Weekly composite chlorophyll *a* concentration in the study area for 1–8 January **(a)**, 9–16 January **(b)**, 17–24 January **(c)** and 25 January–1 February **(d)** from SeaWIFS imagery. White area indicates no data due to the presence of sea ice or clouds.

BGD
11, 657–690, 2014

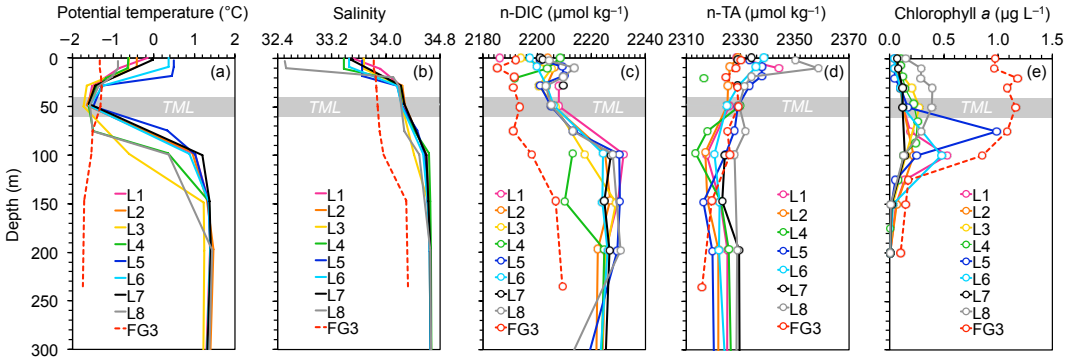

Fig. 6. Vertical profiles of potential temperature **(a)**, salinity **(b)**, salinity-normalized DIC (*n*-DIC) **(c)**, salinity-normalized TA (*n*-TA) **(d)** and chlorophyll *a* concentration **(e)**. Shaded area indicates the temperature minimum layer (TML) for stations L1–8. For FG3, the TML was at 200 m.

BGD
11, 657–690, 2014

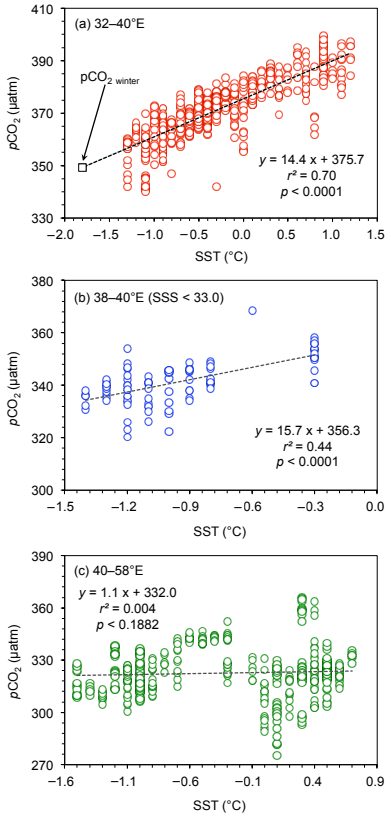

Fig. 7. Relationship between surface-water pCO_2 and SST for 32–40° E **(a)**, the area affected by freshwater input (SSS < 33.0) in 38–40° E **(b)** and 40–58° E **(c)**. Dashed lines are best-fit lines described by the regression equations. Black square in **(a)** indicates surface-water pCO_2 in winter (349.9 µatm) calculated from the carbonate system parameters in the TML.

BGD
11, 657–690, 2014

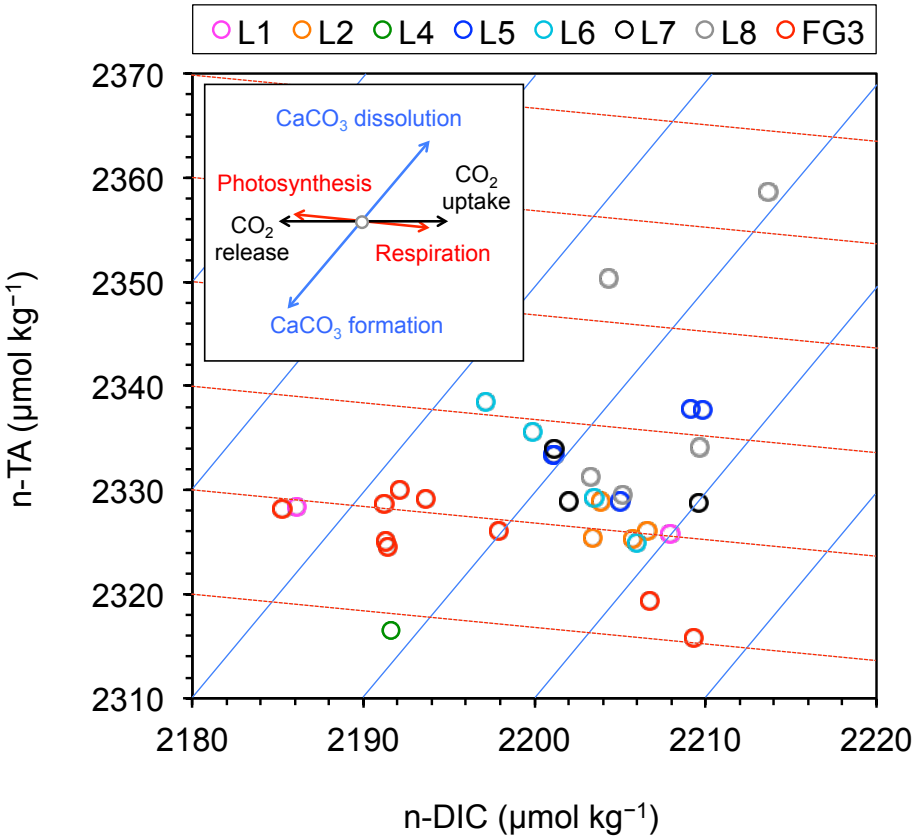

Fig. 8. Relationships between the salinity-normalized DIC (*n*-DIC) and salinity-normalized TA (*n*-TA) for water samples shallower than the TML. The inset indicates theoretical slopes of the different processes affecting *n*-DIC and *n*-TA. Blue and red lines indicate theoretical slopes for $CaCO_3$ dissolution/formation and photosynthesis/respiration, respectively.

BGD
11, 657–690, 2014

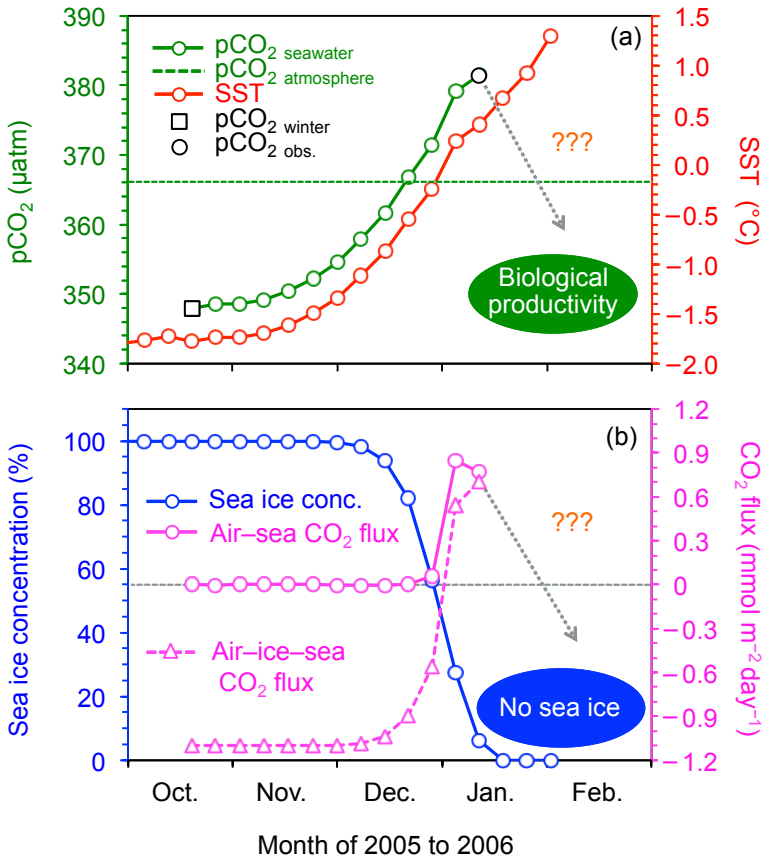

Fig. 9. Seasonal variations of simulated surface-water pCO_2 and SST **(a)** and sea ice concentration and CO_2 fluxes **(b)**. Simulated pCO_2 in **(a)** is constrained by the value in winter (349.9 µatm) calculated from carbonate system parameters in the TML (black square), and the value observed during our observation period (381.5 µatm) (black circle).

BGD
11, 657–690, 2014

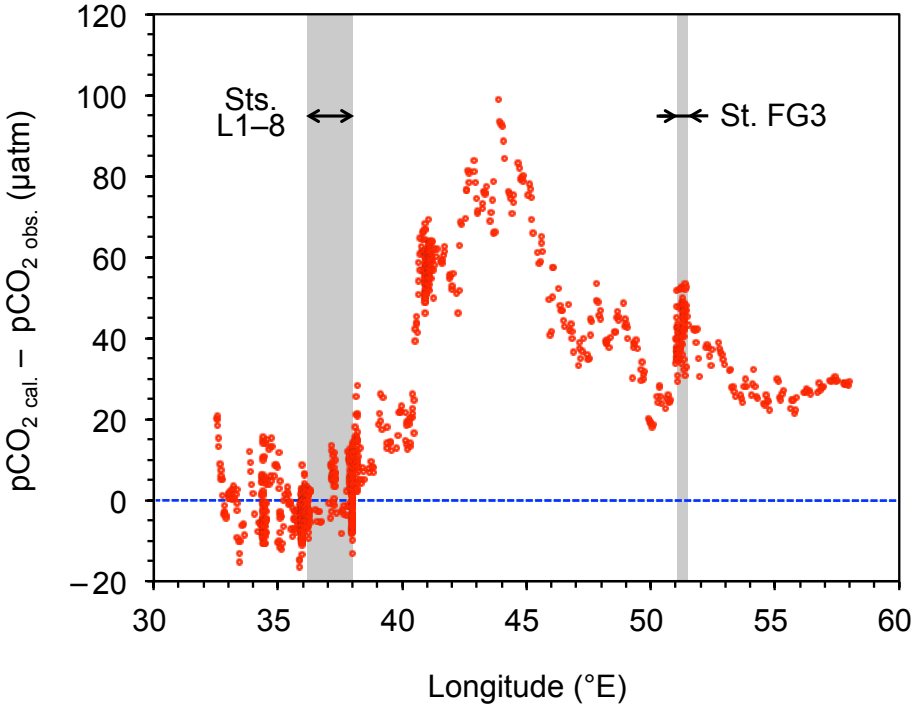

Fig. 10. Longitudinal distribution of the difference between calculated and observed pCO_2. Calculated pCO_2 was computed from n-DIC_{winter} and n-TA_{winter} at the observed SST.

BGD
11, 657–690, 2014